Heterostructures

Deutsche Ausgabe: DOI: 10.1002/ange.201500281
Internationale Ausgabe: DOI: 10.1002/anie.201500281

Solution-Based Synthesis of Layered Intergrowth Compounds of the Homologous $Pb_mBi_{2n}Te_{3n+m}$ Series as Nanosheets**

*Arindom Chatterjee and Kanishka Biswas**

Abstract: *Layered intergrowth compounds in the homologous $Pb_mBi_{2n}Te_{3n+m}$ family are interesting because they are examples of natural heterostructures. We present a simple solution-based synthesis of two-dimensional nanosheets of $PbBi_2Te_4$, $Pb_2Bi_2Te_5$, and $PbBi_6Te_{10}$ layered intergrowth compounds, which are members of the $Pb_mBi_{2n}Te_{3n+m}$ [that is, $(PbTe)_m$-$(Bi_2Te_3)_n$] homologous series. Few-layer nanosheets exhibit narrow optical band gaps (0.25–0.7 eV) with semiconducting electronic-transport properties.*

Use of phase homologies is a fascinating approach to design new materials with predictable composition and structure, such as $A_m(M'_{1+l}Se_{2+l})_{2m}(M''_{2l+n}Se_{2+3l+n})$ (A = alkali metal; M′, M″ = main-group element), $Cs_4(Bi_{2n+4}Te_{3n+6})$, $(BiQX)_2$-$(Ag_xBi_{1-x}Q_{2-2x}X_{2x-1})_{n+1}$ (Q = S, Se; X = Cl, Br; $1/2 \le x \le 1$), and $(Sb_2Te_3)_m(Sb_2)_n$.[1–3] A homology is a series of structures built on the same structural principle with certain modules expanding in various dimensions in regular increments, that is, a series of new compounds with predictable structures can be synthesized through the addition of a layer or row of atoms onto a given module.[4] Several layered intergrowth compounds in the homologous series of the general formula $Pb_mBi_{2n}Te_{3n+m}$ [that is, $(PbTe)_m(Bi_2Te_3)_n$] exist in the PbTe–Bi_2Te_3 phase diagram (Figure 1a),[5] and the layered compounds $PbBi_2Te_4$ and $Pb_2Bi_2Te_5$ in the $Pb_mBi_{2n}Te_{3n+m}$ family are topological insulators.[6–8] This interesting class of compounds can also be viewed as natural heterostructures, which are expected to have low thermal conductivity owing to strong phonon scattering at the interfaces between the layers, and are therefore valuable for thermoelectric applications. The melting points of most of the compounds in the $Pb_mBi_{2n}Te_{3n+m}$ series are incongruent; thus, synthesis of the pure bulk phases through traditional high-temperature solid-state melting techniques is challenging.

A study of the physical properties of layered compounds is interesting because of the directional behavior due to different interlayer (out-of-plane) and intralayer (in-plane) bonding. Ultrathin two-dimensional (2D) nanosheets of layered inorganic analogues of graphene, such as transition-metal dichalcogenides, are fundamentally and technologically intriguing.[9,10] Freestanding single-/few-layer nanosheets of Bi_2Se_3, Bi_2Te_3, and related compounds have shown improved thermoelectric properties relative to their bulk counterparts owing to the presence of enhanced metallic surface states and high carrier mobility.[11–13] Nanosheets of the interesting misfit layer compound SnS_2/SnS and ordered superstructures of SnS_2 and SnS_2/SnS nanotubes have been reported recently by Tenne and co-workers.[14] Few-layer nanosheets of binary chalcogenides, such as MoS_2, WS_2, Bi_2Te_3, and Bi_2Se_3, are mostly synthesized by soft chemical synthesis,[11–13] Li inter-

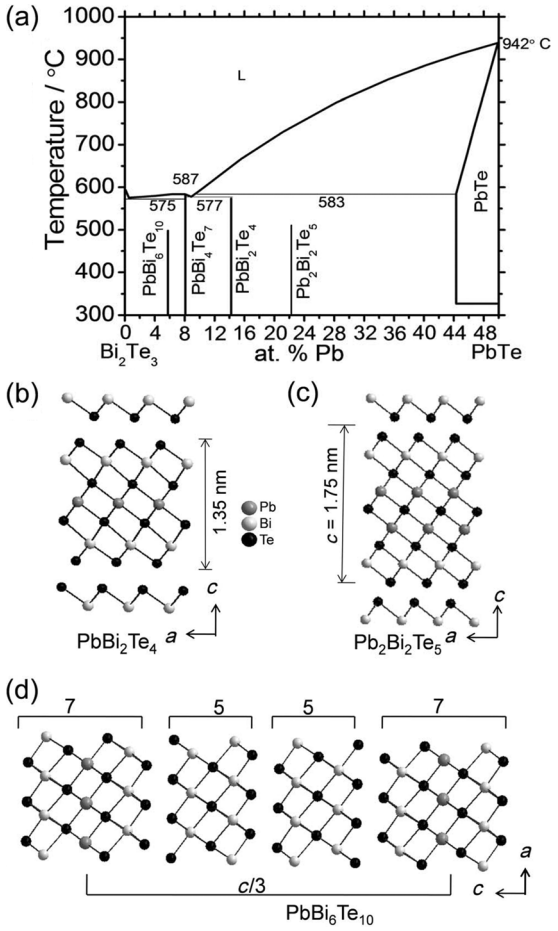

Figure 1. a) Pseudobinary phase diagram of the PbTe–Bi_2Te_3 system showing the presence of several incongruently melting compounds.[5] b, c) Crystal structures of $PbBi_2Te_4$ (b) and $Pb_2Bi_2Te_5$ (c) showing the 1.35 and 1.75 nm thick septuple and nonuple layers, respectively. d) Crystal structure of $PbBi_6Te_{10}$ showing the stacking of quintuple layers of Bi_2Te_3 and septuple layers of $PbBi_2Te_4$.

[*] A. Chatterjee, Dr. K. Biswas
New Chemistry Unit
Jawaharlal Nehru Centre for Advanced Scientific Research (JNCASR)
Jakkur P.O., Bangalore (India)
E-mail: kanishka@jncasr.ac.in
Homepage: http://www.jncasr.ac.in/kanishka/

[**] We thank Prof. C. N. R. Rao for constant support. This research was supported by a Ramanujan Fellowship, SERB and by the Sheikh Saqr Laboratory, JNCASR. We thank Dr. Basavaraj and Dr. J. Ghatak for their help during AFM and TEM measurements, respectively.

Supporting information for this article is available on the WWW under http://dx.doi.org/10.1002/anie.201500281.

calation and exfoliation,[9,10] and liquid-phase exfoliation.[10a,15]

Herein, we demonstrate the first successful synthesis of ultrathin few-layer nanosheets of $PbBi_2Te_4$ ($m=1$, $n=1$), $Pb_2Bi_2Te_5$ ($m=2$, $n=1$), and $PbBi_6Te_{10}$ ($m=1$, $n=3$) in the homologous $Pb_mBi_{2n}Te_{3n+m}$ family by a simple solution-phase method at low temperatures. Nanosheets of homologous $Pb_mBi_{2n}Te_{3n+m}$ compounds exhibit narrow band gaps in the range of approximately 0.25–0.7 eV. $Pb_mBi_{2n}Te_{3n+m}$ nanosheets show low thermal conductivity with semiconducting electronic-transport properties in the temperature range of 300–530 K.

$PbBi_2Te_4$ [that is, $(PbTe)_1(Bi_2Te_3)_1$] in the homologous $Pb_mBi_{2n}Te_{3n+m}$ family is an anisotropic layered material with a tetradymite-type structure ($R\bar{3}m$ space group) and can be described as the intergrowth of PbTe-type (rock-salt) and Bi_2Te_3-type (hexagonal) phases (Figure 1b).[16] $PbBi_2Te_4$ contains septuple layers (SLs), each approximately 1.35 nm thick, which are composed of seven covalently bonded atomic planes [Te^2–Bi–Te^1–Pb–Te^1–Bi–Te^2]. These SLs are periodically stacked along the crystallographic *c*-axis by van der Waals interactions (Figure 1b). The second compound, $Pb_2Bi_2Te_5$ [that is, $(PbTe)_2(Bi_2Te_3)_1$], in the homologous $Pb_mBi_{2n}Te_{3n+m}$ family is also a layered material that crystallizes as a hexagonal structure ($P\bar{3}m1$ space group). $Pb_2Bi_2Te_5$ is formed by the stacking of slabs composed of nine atomic layers (making up a nonuple layer, ca. 1.75 nm thick) with the sequence Te^3–Bi–Te^2–Pb–Te^1–Pb–Te^2–Bi–Te^3, by weak van der Waals interactions along the *c*-axis (Figure 1c). $PbBi_6Te_{10}$ [that is, $(PbTe)_1(Bi_2Te_3)_3$] has a long periodic structure containing 51 layers in the unit cell (Figure 1d displays only one-third of the unit cell).[17] The natural heterostructure of $PbBi_6Te_{10}$ is composed of two types of slabs, a quintuple layer (QL) of Bi_2Te_3 and a septuple layer (SL) of $PbBi_2Te_4$, which are intergrown along the crystallographic *c*-axis with the sequence 755755755 by weak van der Waals interactions (Figure 1d). Each SL slab is sandwiched between two identical QL slabs, whereas each QL slab is sandwiched between dissimilar slabs, one QL and one SL slab.[17]

Ultrathin nanosheets of the pure phases $PbBi_2Te_4$, $Pb_2Bi_2Te_5$, and $PbBi_6Te_{10}$ in the homologous $Pb_mBi_{2n}Te_{3n+m}$ family were synthesized by a simple solution-based technique. We standardized a single procedure for the synthesis of different nanosheets by only varying the nominal compositions of the elemental precursors (i.e. the molar ratio of Pb, Bi, and Te). First, we made a clear precursor solution of Pb by dissolving lead acetate, $Pb(OAc)_2{\cdot}3H_2O$, in oleylamine under vacuum at 100 °C for 1 h, then bismuth neodecenate (the bismuth precursor) was added to the solution. The resulting solution of the metal precursors was heated to 70 °C, and 1-dodecanethiol was added dropwise. The pale-yellow color of the resulting solution indicated the formation of the lead bismuth dodecanethiolate complex.[12] The temperature of the solution was maintained at 70 °C for 5 min to enable the complete formation of the lead bismuth dodecanethiolate complex. Finally, the solution temperature was increased to 90 °C, and a solution of tri-*n*-octylphosphine tellurium (Te-TOP) was immediately injected into it. A black suspension was observed, which was aged for 1 h at 90 °C. (Figure S1 in the Supporting Information shows the color of the reaction mixture at different stages of the reaction.) Black nanosheets of $Pb_mBi_{2n}Te_{3n+m}$ were precipitated out by adding a 1:1 mixture of hexane and ethanol (see the Supporting Information for details of the synthesis).

Our approach to synthesize the pure-phase polycrystalline bulk counterpart of $PbBi_2Te_4$ by the melting of the constituent elements at 700 °C for 10 h and subsequent quenching with water proved to be unsuccessful.[7a] PbTe was identified as an impurity with the $PbBi_2Te_4$ phase (see Figure S2). This impurity is due to the incongruent melting point of $PbBi_2Te_4$. Polycrystalline ingots of $PbBi_2Te_4$ and $PbBi_6Te_{10}$ were synthesized previously by peritectic reactions by heating the required elements above melting temperature and subsequent annealing for several weeks (ca. 1000 h) at 500 °C to avoid unwanted binary phases.[5] The present simple and quick solution-phase synthesis at low temperature (kinetic conditions) enables the stabilization of several pure compounds in the $Pb_mBi_{2n}Te_{3n+m}$ homologous series in the form of nanosheets, which is rather difficult by traditional high-temperature solid-state synthesis. Phase separation was encountered in traditional high-temperature solid-state synthesis owing to the incongruent melting point of $Pb_mBi_{2n}Te_{3n+m}$ compounds. The phase-segregation problem was avoided in the present low-temperature solution synthesis, in which precursor decomposition and bottom-up soft chemical reactions are the key steps, and this process does not involve any melting reactions. Low-temperature synthesis is also essential in arresting pure phases in the form of exotic nanostructures.

Powder X-ray diffraction (PXRD) patterns of the as-synthesized nanosheets could be indexed to pure $PbBi_2Te_4$ (space group $R\bar{3}m$), $Pb_2Bi_2Te_5$ (space group $P\bar{3}m1$), and $PbBi_6Te_{10}$ (space group $R\bar{3}m$; Figure 2a–c). The PXRD patterns of all compounds appeared similar to that of Bi_2Te_3, with slight deviations (see Figure S3), because the fundamental layered structures of homologues $Pb_mBi_{2n}Te_{3n+m}$ are derived from Bi_2Te_3.

The spectroscopically measured band gaps of the $PbBi_2Te_4$ and $PbBi_6Te_{10}$ samples were approximately 0.7 and 0.25 eV, respectively (Figure 2d), thus indicating two distinct compounds. Notably, typical Tyndall light scattering of as-synthesized $PbBi_2Te_4$ nanosheets dispersed in toluene confirmed the colloidal nature of the as-synthesized sample (Figure 2d).

The elemental composition (i.e. the ratio of Pb, Bi, and Te) of as-synthesized $Pb_mBi_{2n}Te_{3n+m}$ nanosheets was determined by three independent characterization techniques: inductively coupled plasma atomic emission spectroscopy (ICP-AES), energy-dispersive X-ray analysis (EDAX), and X-ray photoelectron spectroscopy (XPS). The actual compositions determined by ICP-AES and EDAX were close to the nominal compositions (Table 1), which suggests good control over compositions in the present synthetic process. We also performed EDAX elemental color mapping and elemental line scan analysis on a single nanosheet during scanning transmission electron microscopy (STEM; see below). To further confirm the presence of Pb, Bi, and Te, we performed XPS of $PbBi_2Te_4$ and $Pb_2Bi_2Te_5$ nanosheets (see Fig-

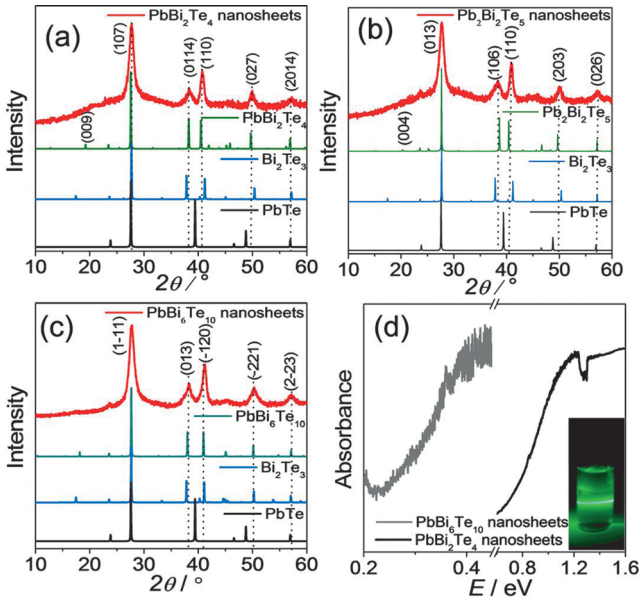

Figure 2. a–c) PXRD patterns of $PbBi_2Te_4$ (ICSD#616936), $Pb_2Bi_2Te_5$ (ICSD#42708), and $PbBi_6Te_{10}$ (ICSD#95551) nanosheets. Dotted lines show the deviation of the PXRD pattern of the nanosheets from that of Bi_2Te_3. d) Electronic absorption spectra of $PbBi_2Te_4$ and $PbBi_6Te_{10}$ nanosheets. The inset in (d) shows the Tyndall light scattering of $PbBi_2Te_4$ nanosheets dispersed in toluene.

Table 1: Nominal composition and experimental composition determined by ICP-AES and EDAX of the as-synthesized nanosheets.

Nominal composition	ICP-AES composition	EDAX composition
$PbBi_2Te_4$	$Pb_{1.06\pm0.02}Bi_{2.13\pm0.03}Te_{3.67\pm0.03}$	$Pb_{1.12\pm0.06}Bi_{1.97\pm0.08}$ $Te_{3.83\pm0.20}$
$Pb_2Bi_2Te_5$	$Pb_{1.67\pm0.02}Bi_{2.23\pm0.02}Te_{4.91\pm0.03}$	$Pb_{2.03\pm0.1}Bi_{2.02\pm0.10}Te_{4.90\pm0.22}$
$PbBi_6Te_{10}$	$Pb_{1.33\pm0.02}Bi_{6.39\pm0.05}Te_{9.31\pm0.08}$	$Pb_{1.08\pm0.04}Bi_{6.28\pm0.20}Te_{9.3\pm0.30}$

ure S4a,b). Two intense peaks at 137.5 and 142.4 eV due to Pb $4f^{7/2}$ and Pb $4f^{5/2}$ were observed, with peak splitting of approximately 5 eV (see Figure S4a). Peaks due to Bi $4f^{7/2}$ and Bi $4f^{5/2}$ appeared at 156.4 and 161.6 eV, respectively. Two more strong peaks due to Te $3d^{5/2}$ and Te $3d^{3/2}$ were observed at 576.7 and 586.8 eV, respectively (see Figure S4a).

Atomic force microscopy (AFM) revealed the ultrathin nature of the $PbBi_2Te_4$ nanosheets. AFM images of free-standing $PbBi_2Te_4$ nanosheets with a thickness corresponding to two SLs (ca. 2.6 nm) and three SLs (ca. 3.9 nm), respectively, were recorded (Figure 3a; see also Figure S5). The lateral dimension of the $PbBi_2Te_4$ nanosheets ranged from 1 μm to several micrometers. A morphology resembling 2D thin sheets was also evident from a field emission scanning electron microscopic (FESEM) image (inset of Figure 3a) and TEM image of $PbBi_2Te_4$ (Figure 3b). A high-resolution TEM (HRTEM) image of a $PbBi_2Te_4$ nanosheet clearly showed a lattice spacing of approximately 0.322 nm, which corresponds to the (107) plane of $PbBi_2Te_4$ (Figure 3c). The selected-area electron diffraction (SAED) pattern recorded for a single-sheet region of $PbBi_2Te_4$ showed a single-crystalline pattern with typical sixfold symmetry (inset of Figure 3c). The SAED pattern for a region in which a few $PbBi_2Te_4$ sheets

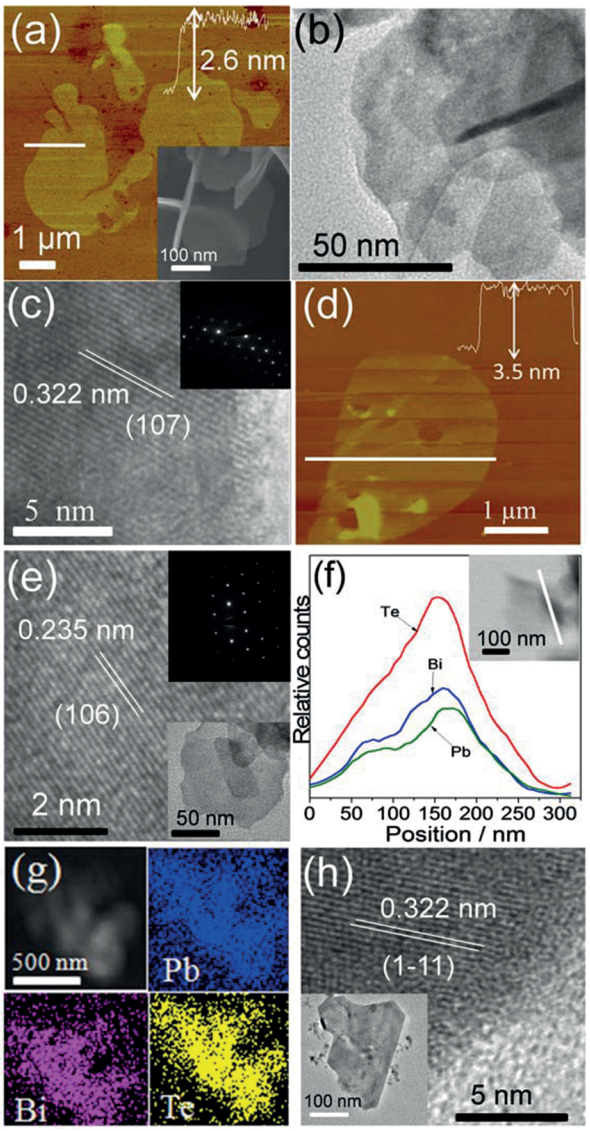

Figure 3. a) AFM image of a $PbBi_2Te_4$ nanosheet. The inset in (a) shows an FESEM image of a $PbBi_2Te_4$ nanosheet. b) TEM image of a $PbBi_2Te_4$ nanosheet. c) HRTEM image of a $PbBi_2Te_4$ nanosheet. The inset in (c) shows the SAED pattern of a single $PbBi_2Te_4$ nanosheet. d) AFM image of a $Pb_2Bi_2Te_5$ nanosheet. e) HRTEM image of a $Pb_2Bi_2Te_5$ nanosheet. The top inset shows the SAED pattern and the bottom inset shows a TEM image of a $Pb_2Bi_2Te_5$ nanosheet. f) EDAX line scan for a single $Pb_2Bi_2Te_5$ nanosheet. The inset in (f) is the corresponding STEM image of the nanosheet. g) EDAX color mapping for Pb, Bi, and Te of a $Pb_2Bi_2Te_5$ nanosheet during STEM imaging. h) HRTEM image of a $PbBi_6Te_{10}$ nanosheet. The inset is the low-magnification TEM image.

were overlapped showed a polycrystalline ring pattern, which can be indexed on the basis of pure $PbBi_2Te_4$ (space group $R\bar{3}m$; see Figure S6). EDAX elemental line scan analysis of a nanosheet of $PbBi_2Te_4$ during scanning transmission electron microscopy (STEM) further confirmed the presence of Pb, Bi, and Te in the expected ratio with single-phase homogeneity (see Figure S7).

In Figure 3d, we show the AFM image of a $Pb_2Bi_2Te_5$ nanosheet with a thickness (ca. 3.5 nm) of two nonuple layers

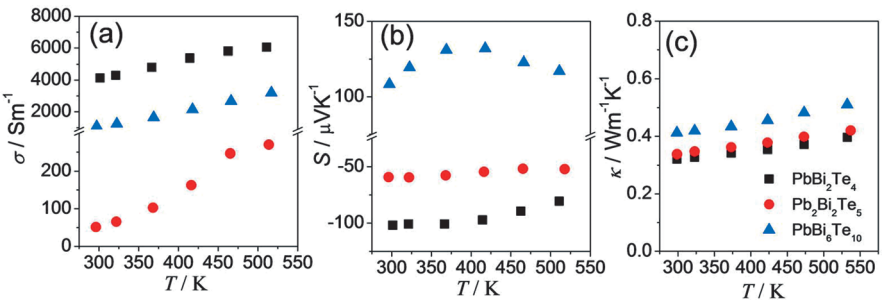

Figure 4. Temperature-dependent a) electrical conductivity (σ), b) Seebeck coefficient (S), and c) thermal conductivity (κ) of $PbBi_2Te_4$, $Pb_2Bi_2Te_5$, and $PbBi_6Te_{10}$ nanosheets.

(NLs, each containing nine atomic layers). TEM images confirmed the 2D thin-sheet morphology of the $Pb_2Bi_2Te_5$ sample (inset of Figure 3e). An HRTEM image of the $Pb_2Bi_2Te_5$ nanosheet clearly showed lattice spacing of approximately 0.235 nm, which corresponds to the (106) plane of $Pb_2Bi_2Te_5$ (Figure 3e; see also Figure S8). The SAED pattern of the $Pb_2Bi_2Te_5$ nanosheets indicates their single-crystalline nature with typical sixfold symmetry (inset of Figure 3e). EDAX elemental line scan analysis on a nanosheet of $Pb_2Bi_2Te_5$ during STEM confirmed the presence of Pb, Bi, and Te in the correct ratio (Figure 3f). The single-phase homogeneity of $Pb_2Bi_2Te_5$ was further confirmed by EDAX elemental mapping on a nanosheet of $Pb_2Bi_2Te_5$ during STEM imaging (Figure 3g). A TEM image of the $PbBi_6Te_{10}$ sample also indicated a 2D thin-sheet morphology (inset of Figure 3h). An HRTEM image of the $PbBi_6Te_{10}$ nanosheet showed a lattice spacing of approximately 0.322 nm, which corresponds to the $(1\bar{1}1)$ plane of $PbBi_6Te_{10}$ (Figure 3h; see also Figure S8).

The narrow band gap and multilayer structure of $Pb_mBi_{2n}Te_{3n+m}$ nanosheets motivated us to measure their temperature-dependent electronic- and phonon-transport properties preliminarily (Figure 4). To measure their thermoelectric properties, we removed the organic capping ligands by treating as-synthesized samples with hydrazine and chloroform (see Figure S9). The surface-cleaned nanosheets were hot-pressed under vacuum in a graphite die by applying a pressure of 20 MPa at 623 K for 30 min. The density of the hot-pressed sample was about 95% of the theoretical density. Simultaneous measurements of electrical conductivity (σ) and the Seebeck coefficient (S) were carried out under a helium atmosphere from 300 to 530 K in a ULVAC ZEM 3 instrument. At room temperature, the σ values for $PbBi_2Te_4$, $Pb_2Bi_2Te_5$, and $PbBi_6Te_{10}$ samples were 4130, 51, and 1073 $S\,m^{-1}$, respectively (Figure 4a). The σ value increased with increasing temperature, thus indicating the semiconducting nature of $Pb_mBi_{2n}Te_{3n+m}$ nanosheets. The negative Seebeck coefficient of the $PbBi_2Te_4$ and $Pb_2Bi_2Te_5$ nanosheets indicates n-type semiconducting behavior, whereas the positive Seebeck coefficient of $PbBi_6Te_{10}$ indicates p-type semiconducting behavior. The room-temperature S values for the $PbBi_2Te_4$, $Pb_2Bi_2Te_5$, and $PbBi_6Te_{10}$ samples were −102, −60, and 109 $\mu V\,K^{-1}$, respectively (Figure 4b). Although electronic-transport measurement data for bulk $Pb_mBi_{2n}Te_{3n+m}$ phases are rare,[18] we compare the electronic-transport data of present $Pb_mBi_{2n}Te_{3n+m}$ nanosheets with those of their bulk counterparts in Table S1 of the Supporting Information. Nanosheets of $Pb_mBi_{2n}Te_{3n+m}$ exhibited low thermal-conductivity (κ) values ranging from 0.33 to 0.52 $W\,mK^{-1}$ in the 300–530 K temperature range (Figure 4c). Low κ values were observed owing to phonon scattering as a result of interfaces between the layers of long periodic structure. Pristine $PbBi_2Te_4$ and $PbBi_6Te_{10}$ nanosheet samples exhibited the highest thermoelectric figures of merit (zT) of approximately 0.06 and 0.04 at 415 and 520 K, respectively. These values are comparable to those of other binary metal chalcogenide nanosheets.[13b]

In conclusion, we have described the synthesis of ultrathin nanosheets of homologous $Pb_mBi_{2n}Te_{3n+m}$ layered compounds by a low-temperature solution-based method. The stabilization of the pure-phase compounds in the $Pb_mBi_{2n}Te_{3n+m}$ family in the form of nanosheets is attributed to the kinetic low-temperature synthesis and the influence of the nanoscale regime, and is rather difficult to achieve by high-temperature solid-state bulk-phase synthesis. Members of the $Pb_mBi_{2n}Te_{3n+m}$ family are examples of natural superlattice structures. These nanosheets exhibit narrow optical band gaps and semiconducting electronic-transport properties. The long periodic intergrowth structure of these materials leads to low thermal conductivity. Control of the ratio of the different substructures may enable the modulation of their electronic structure and better control of their charge-transport properties.

Keywords: intergrowth compounds · nanosheets · nanostructures · semiconductors · ternary metal chalcogenides

How to cite: *Angew. Chem. Int. Ed.* **2015**, *54*, 5623–5627
Angew. Chem. **2015**, *127*, 5715–5719

[1] M. G. Kanatzidis, *Acc. Chem. Res.* **2005**, *38*, 361–370.
[2] a) M. Ruck, P. F. P. Poudeu, *Z. Anorg. Allg. Chem.* **2008**, *634*, 482–490; b) M. Ohta, D. Y. Chung, M. Kuniib, M. G. Kanatzidis, *J. Mater. Chem. A* **2014**, *2*, 20048–20058.
[3] a) P. F. P. Poudeu, M. G. Kanatzidis, *Chem. Commun.* **2005**, 2672–2674; b) R. Atkins, M. Dolgos, A. Fiedler, C. Grosse, S. F. Fischer, S. P. Rudin, D. C. Johnson, *Chem. Mater.* **2014**, *26*, 2862–2872.
[4] A. Mrotzek, M. G. Kanatzidis, *Acc. Chem. Res.* **2003**, *36*, 111–119.
[5] L. E. Shelimova, O. G. Karpinskii, P. P. Konstantinov, E. S. Avilov, M. A. Kretova, I. Y. Nikhezina, V. S. Zemskov, *Inorg. Mater.* **2010**, *1*, 83–91.
[6] K. Yang, W. Setyawan, S. Wang, M. B. Nardelli, S. Curtarolo, *Nat. Mater.* **2012**, *11*, 614–619.
[7] a) K. Kuroda, H. Miyahara, M. Ye, S. V. Eremeev, Y. M. Koroteev, E. E. Krasovskii, E. V. Chulkov, S. Hiramoto, C. Moriyoshi, Y. Kuroiwa, K. Miyamoto, T. Okuda, M. Arita, K. Shimada, H. Namatame, M. Taniguchi, Y. Ueda, A. Kimura, *Phys. Rev. Lett.* **2012**, *108*, 206803; b) K. Nakayama, K. Eto, Y. Tanaka, T. Sato, S. Souma, T. Takahashi, K. Segawa, Y. Ando, *Phys. Rev. Lett.* **2012**, *109*, 236804.

[8] I. V. Silkin, Y. M. Koroteev, S. V. Eremeev, G. Bihlmayer, E. V. Chulkov, *JETP Lett.* **2011**, *94*, 217 – 221.
[9] a) H. S. S. R. Matte, A. Gomathi, A. K. Manna, D. J. Late, R. Datta, S. K. Pati, C. N. R. Rao, *Angew. Chem. Int. Ed.* **2010**, *49*, 4059 – 4062; *Angew. Chem.* **2010**, *122*, 4153 – 4156; b) C. Tan, Z. Zheng, X. Huang, X. Rui, X. J. Wu, B. Li, Z. Luo, J. Chen, B. Chen, Q. Yan, H. Zhang, *Angew. Chem. Int. Ed.* **2015**, *54*, 1841 – 1845; *Angew. Chem.* **2015**, *127*, 1861 – 1865; c) X. Huang, Z. Y. Zheng, H. Zhang, *Chem. Soc. Rev.* **2013**, *42*, 1934 – 1946.
[10] a) V. Nicolosi, M. Chhowalla, M. G. Kanatzidis, M. S. Strano, J. N. Coleman, *Science* **2013**, *340*, 1420; b) M. Chhowalla, H. S. Shin, G. Eda, L.-J. Li, K. P. Loh, H. Zhang, *Nat. Chem.* **2013**, *5*, 263 – 275; c) C. Tan, H. Zhang, *Chem. Soc. Rev.* **2015**, DOI: 10.1039/C4CS00182F; d) H. Li, J. Wu, Z. Yin, H. Zhang, *Acc. Chem. Res.* **2014**, *47*, 1067 – 1075; e) X. Huang, C. Tan, Z. Yin, H. Zhang, *Adv. Mater.* **2014**, *26*, 2185 – 2204; f) Z. Zeng, Z. Yin, X. Huang, H. Li, Q. He, G. Lu, F. Boey, H. Zhang, *Angew. Chem. Int. Ed.* **2011**, *50*, 11093 – 11097; *Angew. Chem.* **2011**, *123*, 11289 – 11293.
[11] Y. Sun, H. Cheng, S. Gao, Q. Liu, Z. Sun, C. Xiao, C. Wu, S. Wei, Y. Xie, *J. Am. Chem. Soc.* **2012**, *134*, 20294 – 20297.
[12] J. S. Son, M. K. Choi, M.-K. Han, K. Park, J.-Y. Kim, S. J. Lim, M. Oh, Y. Kuk, C. Park, S.-J. Kim, T. Hyeon, *Nano Lett.* **2012**, *12*, 640 – 647.
[13] a) Y. Min, J. W. Roh, H. Yang, M. Park, S. I. Kim, S. Hwang, S. M. Lee, K. H. Lee, U. Jeong, *Adv. Mater.* **2013**, *25*, 1425 – 1429; b) M. K. Jana, K. Biswas, C. N. R. Rao, *Chem. Eur. J.* **2013**, *19*, 9110 – 9113; c) A. Chatterjee, S. N. Guin, K. Biswas, *Phys. Chem. Chem. Phys.* **2014**, *16*, 14635 – 14639.
[14] a) G. Radovsky, R. P. Biro, R. Tenne, *Chem. Mater.* **2014**, *26*, 3757 – 3770; b) G. Radovsky, R. P. -Biro, M. Staiger, K. Gartsman, C. Thomsen, T. Lorenz, G. Seifert, R. Tenne, *Angew. Chem. Int. Ed.* **2011**, *50*, 12316 – 12320; *Angew. Chem.* **2011**, *123*, 12524 – 12528; c) G. Radovsky, R. P. Biro, D. G. Stroppa, L. Houben, R. Tenne, *Acc. Chem. Res.* **2014**, *47*, 406 – 416.
[15] J. N. Coleman, M. Lotya, A. O'Neill, S. D. Bergin, P. J. King, U. Khan, K. Young, A. Gaucher, S. De, R. J. Smith, I. V. Shvets, S. K. Arora, G. Stanton, H.-Y. Kim, K. Lee, G. T. Kim, G. S. Duesberg, T. Hallam, J. J. Boland, J. J. Wang, J. F. Donegan, J. C. Grunlan, G. Moriarty, A. Shmeliov, R. J. Nicholls, J. M. Perkins, E. M. Grieveson, K. Theuwissen, D. W. McComb, P. D. Nellist, V. Nicolosi, *Science* **2011**, *331*, 568.
[16] L. Zhang, D. J. Singh, *Phys. Rev. B* **2010**, *81*, 245119.
[17] O. G. Karpinskii, L. E. Shelimova, E. S. Avilov, M. A. Kretova, V. S. Zemskov, *Inorg. Mater.* **2002**, *38*, 17 – 24.
[18] L. E. Shelimova, O. G. Karpinskii, P. P. Konstantinov, E. S. Avilov, M. A. Kretova, V. S. Zemskov, *Inorg. Mater.* **2004**, *40*, 451 – 460.

Received: January 13, 2015
Revised: February 19, 2015
Published online: March 12, 2015

